Density functional theory based calculation of small-polaron mobility in hematite

Nicole Adelstein,[1,*] Jeffrey B. Neaton,[2,3,4] Mark Asta,[5,6] and Lutgard C. De Jonghe[5,6,†]

[1]*Condensed Matter and Materials Division, Lawrence Livermore National Laboratory, Livermore, California 94550, USA*

[2]*Molecular Foundry, Materials Sciences Division, Lawrence Berkeley National Laboratory, Berkeley, California 94720, USA*

[3]*Department of Physics, University of California, Berkeley, Berkeley, California 94720, USA*

[4]*Kavli Energy NanoSciences Institute at Berkeley, Berkeley, California 94720, USA*

[5]*Materials Science and Engineering Department, University of California, Berkeley, Berkeley, California 94720, USA*

[6]*Materials Sciences Division, Lawrence Berkeley National Laboratory, Berkeley, California 94720, USA*

(Received 16 October 2013; published 11 June 2014)

The mobility of electron small polarons in hematite, α-Fe_2O_3, is calculated by density functional theory within the generalized gradient approximation including Hubbard U corrections. Our work goes beyond previous computational investigations of this system by computing both the prefactor and activation energies for adiabatic polaron transport. The results obtained using a Hubbard U value of 4.3 eV yield a calculated value of the room-temperature basal plane mobility of 0.009 S*cm^2/s, which compares to within an order of magnitude with experimental measurements. Further, the values of the electronic-coupling parameter in the Marcus theory for small-polaron transport are estimated from DFT + U calculations of the defect energy levels in the stable and saddle-point configurations. Our results predict an adiabatic polaron transfer, in good agreement with previous wave function based calculations.

DOI: 10.1103/PhysRevB.89.245115 PACS number(s): 71.15.Mb, 71.38.−k, 71.10.Fd, 66.30.Lw

I. INTRODUCTION

Predictive modeling of the mobility of polarons in transition metal oxides and other ionic systems is an active field, as controlling conductivity in these materials can improve the performance of many technologies such as batteries [1,2], thermoelectrics [3], photovoltaics [4,5], catalysts for water splitting [6–8], solid-oxide fuel cells [9], and oxidation of organic compounds [10]. In many transition-metal oxides, charge transport occurs through the hopping of small polarons [11,12], i.e., highly localized electrons or holes that are self-trapped by the polarization of the surrounding lattice. Small polaron mobilities in these systems are typically modeled within the framework of Marcus theory [13], with the associated parameters derived from quantum-mechanical calculations employing either wave function based calculations on clusters [14,15] or density functional theory based calculations (DFT) on periodic supercells [1,16,17].

Within Marcus theory, in limiting cases where the transfer falls into the nominally adiabatic or nonadiabatic regimes, the electron transfer rate, τ, can be expressed as

$$\tau = A \exp\left(\frac{-\Delta E^{\ddagger}}{kT}\right), \tag{1}$$

where A is a preexponential factor, $\Delta E^{\ddagger}$ denotes the activation energy barrier, T is temperature, and k is the Boltzmann constant. For electron transfer between equivalent ions, there is assumed no free energy change, so only the energy barrier is necessary to consider when evaluating the rate.

The energy barrier $\Delta E^{\ddagger}$ is determined by the nature of the hopping mechanism, which can be roughly ascertained by evaluating the Landau-Zener approximation for the diabatic electron transfer probability. Following Ref. [18], this probability is redefined as the adiabadicity parameter, γ:

$$\gamma = \frac{1}{h\nu_{\text{eff}}}\left(\frac{\pi}{4\Delta E_{\text{ad}} kT}\right)^{\frac{1}{2}} \text{V}_{AB}^2. \tag{2}$$

In Eq. (2), ΔE_{ad} is the adiabatic activation energy, h is Planck's constant, and ν_{eff} is the effective frequency for motion along the reaction coordinate, which can be estimated from a typical phonon frequency in the material. The high temperature limit is assumed, such that the electronic coupling matrix element, V_{AB}, is a measure of the overlap integral between states A and B. Note that in the low temperature limit vibronic factors are necessary to capture the coupling between the electron and the lattice at the transition state (TS).

The probability of charge transfer is $1 - \exp[-\gamma]$ and, if γ is much less than 1, the transfer is nonadiabatic and the rate is governed by Fermi's golden rule. In this weak coupling regime, the Born-Oppenheimer approximation does not hold, as the electron remains localized on the initial ion on the time scale of typical phonon cycles. On the other hand, if the electronic coupling is large compared to the activation energy barrier, the transfer can be considered adiabatic. In this case, the adiabatic activation energy barrier, ΔE_{ad}, decreases by V_{AB} from the diabatic (more generally, nonadiabatic) activation energy barrier, ΔE_{dia}, such that $\Delta E_{\text{ad}} = \Delta E_{\text{dia}} - \text{V}_{AB}$, as illustrated in Fig. 1. Thus knowledge of V_{AB} and either ΔE_{dia} or ΔE_{ad} allows one to determine the nature of the transfer process through Eq. (2).

The calculation of nonadiabatic activation energy barriers has traditionally been undertaken using wave function based quantum chemistry methods, where the electronic wave function can be held constant while the atom positions are interpolated between the reactant and product configurations. Small polarons hop between these two potential energy

*adelstein1@llnl.gov

†Current address: PolyPlus Battery Company, Berkeley, California 94710, USA.

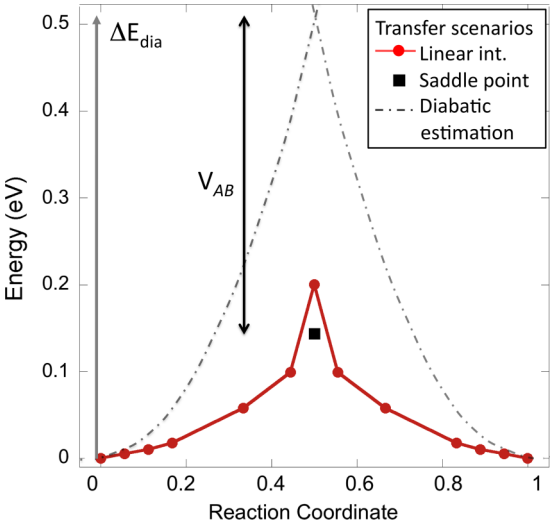

FIG. 1. (Color online) Plot showing the results for adiabatic and nonadiabatic energy barriers for polaron hopping in α-Fe_2O_3, as calculated by the DFT + U method and the approach described in the text. The dashed lines show harmonic energy curves with the calculated nonadiabatic energy barrier (ΔE_{dia}), given by the intersection of the curves, corresponding to the value calculated in this work. The red line shows the adiabatic energies along a reaction path defined by linearly interpolating the atomic positions between the initial and final polaron states. The black symbol gives a refined value for the adiabatic activation energy barrier (ΔE_{ad}) defined by relaxing the approximate saddle-point geometry determined by linear interpolation. The difference between ΔE_{dia} and ΔE_{ad} corresponds to the magnitude of the electron coupling matrix element, V_{AB}. The images from the linear interpolation and the relaxed saddle point are calculated for the 30-atom unit cell with $U = 4.3$ eV.

minima, which can be modeled as intersecting harmonic wells centered at the reactant and product states. Wave function based methods can also be used to compute V_{AB} and many researchers have used cluster models in order to implement Hartree-Fock based methods in the calculations of these parameters and associated polaron mobilities [19–24].

Adiabatic charge transfer implies the validity of the Born-Oppenheimer approximation, and DFT-based methods have been employed for modeling polaron transfer in this limiting regime, as described below. A main drawback of DFT within local or semilocal approximations for the exchange-correlation potential is the failure to correctly describe highly localized electrons such as d electrons in transition metals or f electrons in lanthanides and actinides due to the self-interaction error and missing correlation. The addition of a Hubbard U correction [25] is an approximate way to overcome these limitations; the magnitude of the Hubbard U parameters are typically determined empirically or self-consistently either with linear response theory [26] or through the calculation of Coulomb and exchange integrals using unrestricted Hartree-Fock theory [27]. Both DFT + U [1,2,17,28–31] and constrained DFT [32,33] methods have been used to determine adiabatic activation energy barriers for polaron transport. The advantage of such approaches stems from their computational efficiency, which enables the use of large supercells that can accurately capture the nature of the lattice distortions that may arise from small-polaron formation and migration. A limitation of this approach in most implementations is that polaron transport is implicitly assumed to be adiabatic in nature, and methods for checking the validity of this assumption within DFT-based frameworks have not been presented, to the best of our knowledge. Further, the results can vary significantly with changes in the magnitude of the U parameter, and in some cases this sensitivity is not examined in detail.

In the present work we employ a DFT + U approach to study polaron transport in hematite, α-Fe_2O_3. Our interest in α-Fe_2O_3 stems from the importance of this compound in energy technologies and geochemistry, which has motivated extensive experiments [6,34–36] and computational studies [15,20,37–44] of its defect properties, optical excitations, and electronic conductivity. As a consequence, experimentally derived values for the electronic mobilities are available for this compound [45], allowing a direct comparison between measurements and calculations to examine the accuracy of the DFT + U approach. To enable such a direct comparison, in the current study we compute the attempt frequency for adiabatic polaron transport in addition to the activation energy for polaron hopping.

The availability of previously published computational work employing wave function based cluster calculations [19,46] for α-Fe_2O_3 enables a direct comparison between results obtained with these methods and the independent DFT + U calculations performed in the present study. For comparisons with previous calculations, we present in this work a method for estimating the magnitude of the electronic coupling matrix element (V_{AB}) within the DFT + U approach, based on an analysis of the self-consistent electronic energy levels computed for the ground- and transition-state geometries.

The remainder of this paper is organized as follows. In the next section, we describe the details of the application of the DFT + U approach to determining the parameters entering into the Marcus theory method of calculation of electron small-polaron mobilities. The results for hematite are presented in the following section, including a discussion of the sensitivity of the calculated mobilities to the choice of the Hubbard U parameter, along with a comparison of the present results with previous calculations and measurements.

II. COMPUTATIONAL METHODS

Hematite (α-Fe_2O_3) has the corundum-type structure with the $R\bar{3}c$ space group, in which the oxygen ions are hexagonal close-packed and form stacked octahedra, as in Fig. 2. The hexagonal unit cell contains six formula units, while the primitive cell is rhombohedral with two formula units. The Néel temperature is 953 K [47], so hematite is antiferromagnetic at room temperature with the Fe spins coupled ferromagnetically in the basal planes above the Morin temperature of 250 K.

Hematite is a native n-type material and in this work we will consider the properties of electron small polarons. Henceforth, we will therefore use the term "polaron" to refer to the electron small polaron. In hematite, polaron hopping is expected to be much more facile between iron atoms with the same spin, and conductivity in the basal plane is greater than along the c axis at room temperature [48,49]. In order to compare with

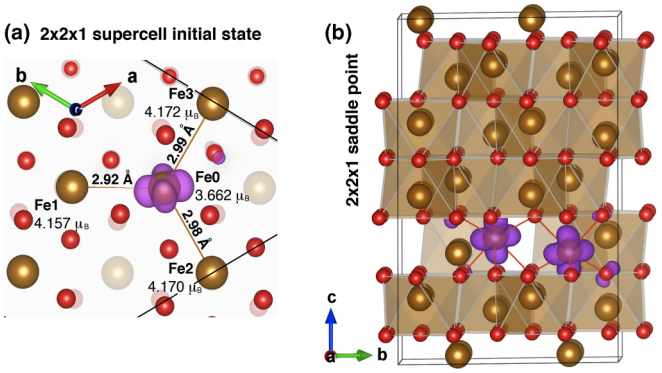

FIG. 2. (Color online) (a) **c**-axis projection of the $2 \times 2 \times 1$ supercell of α-Fe_2O_3 shows the initial ground state of the polaron and its three nearest neighbors in the basal plane: Fe1, Fe2, and Fe3 (Fe ions in gold) along with the associated bond lengths and local magnetic moments. The charge density of the Fe^{2+} small polaron is illustrated by the purple isosurface. The black lines give a sense of the **a** and **b** lattice vectors and the red oxygen ions show hexagonal close packing. (b) The same supercell viewed along the **a** axis at the saddle point for a hop between nearest neighbors shows the polaron is delocalized over the initial and final Fe ions and a few oxygen ions. (These images were made with VESTA [50].)

room-temperature mobility measurements, in our calculations we use the antiferromagnetic structure above the Morin temperature. We focus on transfer of an electron small polaron (Fe^{2+}) to one of its nearest Fe^{3+} neighbors in the basal plane. In Fig. 2(b), the two Fe ions highlighted with the polaron's charge density are nearest neighbors.

A. Activation energy

Our approach for calculating the adiabatic activation energy barriers starts by determining the ground state of the polaron and continues by calculating the relaxed saddle-point energy. The ground-state configuration is determined by adding an extra electron to a supercell (and an accompanying positive background) with periodic boundary conditions and then allowing the ions and volume to relax. In order to converge to a state corresponding to a localized polaron on a specific Fe site, we intentionally break the symmetry of the bulk crystal structure by manually moving one oxygen ion on the order of 0.01 Å away from its "nearest" Fe atom, lifting degeneracies associated with the spatial location of the polaron. When the cell is allowed to relax, polaron formation is reflected by a change in the magnetic moment on the Fe atoms and change in neighboring bond lengths, as described further below. The localization of the electron can also be observed by plotting the charge density associated with the extra electron and by analyzing the electronic density of states (DOS).

The ground-state configuration is represented by the state labeled **0** in Fig. 1, which shows a plot of the energy as a function of reaction coordinate for transfer of a polaron to a neighboring equivalent site, labeled **1**. The initial and final states for the polaron in the same ferromagnetically ordered basal plane are identical by symmetry. Thus, once the ground-state configuration (ionic positions) is determined for the polaron on the initial Fe site, a simple translational operation on the ionic positions can be used to obtain the polaron configuration in the final state.

Figure 1 shows three different scenarios for modeling polaron transfer along the reaction coordinate. The first is illustrated by the dashed gray lines, which schematically represent harmonic potential energy wells centered on the sites **0** and **1** and describe the change in energy as a function of the ionic positions along a path where the electron remains localized on one of the two sites. The intersection of the harmonic potentials for the polaron localized on sites **0** and **1** gives the nonadiabatic activation energy barrier (labeled ΔE_{dia} in Fig. 1). The magnitude of ΔE_{dia} is estimated in the current work from the sum of the adiabatic activation energy (ΔE_{ad}) and an estimate of the magnitude of the electron coupling matrix element (V_{AB}) obtained as described below.

In the second scenario, the red lines with circles represent a commonly employed approximation to the adiabatic activation energy (e.g., Ref. [17]) derived by linearly interpolating the ionic positions between states **0** and **1** and computing the energies for self-consistent charge densities on the Born-Oppenheimer surface corresponding to these different ionic configurations. In what follows we will use the symbol $\Delta \tilde{E}_{\mathrm{ad}}$ to denote the difference in energy between the points **0** and **0.5**, the approximate adiabatic TS, on the Born-Oppenheimer surface obtained from linear interpolation of ionic positions. In the final scenario, the black solid square at the transition state represents a refined estimate of the adiabatic activation energy, derived in this work by performing a force-based relaxation of the ions to the nearest extremum starting from the transition state geometry approximated by linear interpolation.

B. Attempt frequency and mobility

As will be reviewed below, nearest-neighbor polaron transfer in hematite is adiabatic in nature. To enable a comparison between measured and calculated values of the polaron mobility, we compute the preexponential term (A) in Eq. (1), using calculated phonon frequencies for the initial and saddle-point configurations. Specifically, we compute the prefactor from the relation $A = n\tau_0$, where n is the number of equivalent neighbors and τ_0 is the attempt frequency, which is computed in the present work within the framework of harmonic transition-state theory (e.g., Ref. [51]).

The classical attempt frequency in harmonic transition-state theory can be written as the ratio of the product of the vibrational modes at the ground and transition states (excluding the three translational modes and the additional unstable mode at the TS). This classical expression is derived assuming the temperature is higher than the Debye temperature, which is approximately 480 K [52] in hematite. Since we are interested in comparing to experimental measurements at room temperature, we employ the full quantum-mechanical expression for the vibrational free energy in the saddle and ground-state configurations, accounting for the temperature-dependent occupations of the phonon modes. This gives the following expression for the attempt frequency

(e.g., [53]):

$$\tau_0 = \frac{kT}{h} \exp\left(\sum_{\mathrm{Re}[m]} \ln\left[2 \sinh\left(x_m^{GS}\right)\right] - \sum_{\mathrm{Re}[m]} \ln\left[2 \sinh\left(x_m^{TS}\right)\right] \right), \quad (3)$$

where the sums are over the real values of x_m, which equals the calculated phonon frequencies, ν_m, times $h/(2kT)$. As described in the Results section below, this expression leads to a significantly higher attempt frequency than the classical expression at room temperature.

From the calculated value of $A = n\tau_0$, and the activation energy for hopping ΔE_{ad}, the adiabatic transition rate τ can be computed from Eq. (1), and used to compute the diffusion coefficient, D, and the mobility, μ, through the standard relations:

$$\mu = \frac{eD}{kT} = \frac{e}{kT}\frac{a^2\tau}{4}, \quad (4)$$

where a is the electron transfer distance, e is the charge of the electron, and the value of 4 in the denominator reflects 2D mobility.

While we report one value for the 2D mobility in the basal plane, in reality the mobility is a tensor, which characterizes the anisotropy of diffusion along different axes of the crystal. In order to compute the mobility in a single crystal material one would have to determine the activation energy and rate for charge transfer along each of the different axes of the crystal. In what follows we report calculated values of the mobility only in the basal plane. These computational results should thus be viewed as an upper bound to measurements made on polycrystalline samples, which would average over different crystallographic directions.

C. Electronic coupling

In applications of DFT + U methods to the calculation of polaron activation energy barriers it is commonly assumed that the hopping process is adiabatic in nature [1,30,31]. As described in this section, the validity of this assumption can be checked from a consideration of the ground-state and saddle-point electronic structure. Specifically, we can determine the adiabaticity parameter [γ, defined in Eq. (2)] if we know the adiabatic activation energy barrier and the electronic coupling.

We estimate the electronic coupling matrix element along the lines of the Mulliken-Hush formalism within Marcus theory, as described in Ref. [54]. In the Mulliken-Hush formula, ΔE_{12} is the energy difference between the adiabatic bonding and antibonding electronic states at the TS, which is related to the parameter V_{AB} as follows:

$$\mathrm{V}_{AB} = \tfrac{1}{2}\Delta E_{12}. \quad (5)$$

This energy difference (ΔE_{12}) will be estimated from the positions of the two gap states, above and below the Fermi energy, at the TS. In order to employ the Mulliken-Hush formalism, the bonding and antibonding states in the TS ionic configuration must fall in the gap and should be linear combinations of the initial and final polaron states. From an analysis of the charge density in the ground state and transition state configurations, this conjecture is viewed to be reasonable.

We emphasize that since we are using an unoccupied state from a ground-state theory (DFT), we are only *estimating* V_{AB} to determine the adiabaticity of the polaron tranfer, rather than calculating an exact value of the electronic coupling parameter. When determining the adiabaticity of a charge-transfer process in this manner, the uncertainty in calculating ΔE_{12} should be considered since DFT is known to underestimate band gaps. This uncertainly is reduced to some extent in our calculations by choosing the appropriate value of the Hubbard U parameter which improves the calculated band gap. We also note that the energy levels of shallow defect states have been reported, in certain cases, to be more accurate relative to the band edge than those in the center of the gap [55]. Since the polaron gap states are close to the band edges for nearest-neighbor transfer, we can be more confident in our estimation of the adiabaticity.

D. Calculation details

The present calculations make use of DFT within the generalized-gradient approximation (GGA) functional of Perdew, Becke, and Ernzerhof (PBE) [56] as implemented in the Vienna Ab Initio Simulation Package (VASP) [57,58]. Within VASP, the projector-augmented-wave (PAW) method [59] is employed using the PBE-PAW potentials with eight valence electrons for Fe and six valence electrons for O. The electronic wave functions are expanded in a plane wave basis set with a 650 eV energy cutoff. We use a $2 \times 2 \times 2$ k-point mesh for hexagonal $2 \times 2 \times 1$ supercells and a $4 \times 4 \times 2$ k-point mesh for 30 atom hexagonal cells. Based on convergence tests, we estimate that the energy for both cells are converged with respect to k points to within 10^{-4} eV. For total energy and relaxation calculations, a Gaussian smearing of the electronic states with a width of 0.03 eV is used, while density of state calculations employ the tetrahedron method of k-point generation with Bloch corrections [59] for sampling the Brillouin zone. In the structural relaxations, the energy is optimized with respect to atomic positions until the forces on the ions in the bulk unit cells are converged to 0.001 eV/Å and the forces in the cells containing polaron defects are converged to 0.01 eV/Å. The criterion for convergence of the self-consistent charge density was a tolerance on the energy change of 10^{-7} eV.

In all calculations we make use of the rotationally invariant form of the DFT + U approach introduced by Dudarev *et al.* [25], coupled with the PBE-GGA. In the formalism of Dudarev *et al.*, the Hubbard model parameters, U and J, are not independent, and the energy depends only on the parameter $U_{\mathrm{effective}} = U - J$. In the text above and below we refer to the value of $U_{\mathrm{effective}}$ simply as U. An important issue in the present application of the DFT + U approach is the choice of the magnitude of the effective Hubbard U parameter. In order to assess the sensitivity of the calculated results to changes in the value of U, we calculated the activation energy barrier from linear interpolation ($\Delta \tilde{E}_{\mathrm{ad}}$) for transfer to the ions labeled Fe1 and Fe2 in Fig. 2, using the $2 \times 2 \times 1$, 120 atom supercell with values of U ranging from 3.1 to 6.3 eV. These cover the range of values employed in previous DFT + U

studies of hematite [38,60,61], maghemite (γ-Fe_2O_3) [62], and magnetite (Fe_3O_4) [36,63–69]. The calculated values of $\Delta\tilde{E}_{ad}$ obtained with values of U in this range increased monotonically from 0.01 eV to 0.47 eV for hopping to Fe1 ions, and from 0.13 to 0.51 eV for hopping to Fe2. The increases in $\Delta\tilde{E}_{ad}$ with U correlate with increases in the local magnetic moment, suggesting a higher degree of electron localization with increasing U. These variations in $\Delta\tilde{E}_{ad}$ correspond to many orders of magnitude variation in the room-temperature mobility of the polaron. It is thus important for what follows to justify the choice of U used in the remainder of this study.

In previous first-principles studies of hematite a value of $U = 4.3$ eV was calculated self-consistently using Fe_2O_3 clusters [27]; this value gave rise to calculated electronic structures comparing favorably to those obtained from higher levels of theory (hybrid functionals and the GW approximation) and from experimental photoemission and inverse-photoemission spectra [38]. A similar result is presented in Ref. [61], which compares the electronic structure of hematite obtained with hybrid functionals with results from a GGA + U calculation by Rollman *et al.* [60]; the authors of Ref. [61] conclude that the choice of $U = 3$ eV used by Rollman *et al.* [60] gives reasonable agreement between DFT + U and hybrid-functional results. Rollman *et al.* [60] themselves arrived at the value of $U = 3$ eV through a comparison of their calculated results with photoemission measurements [70,71]. While values of U in the range of 3 to 4.3 eV give reasonable descriptions of the electronic structure of bulk hematite, the self-consistently calculated value of 4.3 eV compares much better to the measured activation energy than smaller values.

In what follows we will present results obtained with $U = 4.3$ eV and note that the use of a lower value of $U = 3.1$ eV would lead to a significant decrease in the reported activation energy to approximately 0.01 eV, which would increase the polaron hopping rate at room temperature by two orders of magnitude. It is the intent of this work to examine how a parameter-free DFT + U theory performs in the calculation of polaron mobilities, and for this reason we have chosen the value for U derived from Coulombic and exchange overlap integrals in Ref. [27].

III. RESULTS AND DISCUSSION

A. Crystal structure

Table I compares calculated and experimentally measured crystallographic parameters for bulk hematite. As described above, all calculations were obtained using PBE-GGA with Hubbard U corrections and $U = 4.3$ eV. In the calculations Fe ions were ferromagnetically coupled in the basal planes and antiferromagnetically coupled along the c axis, with a average magnetic moment of $4.17\mu_B$. The Fe ions are high spin with a measured magnetic moment of $4.6\mu_B$ [72]. Consistent with earlier calculations using DFT + U [38,60,73], the present calculations show a good level of agreement with measured crystallographic parameters for bulk hematite, with the lattice constants differing by less than 1% and the Wyckoff positions showing an even better level of agreement.

TABLE I. Calculated and experimental lattice parameters are given in Å. Wyckoff positions are in fractional coordinates. The two Fe-O bond lengths are given in Å and the nearest neighbor O-O angle with Fe is given in degrees. The supercell bond distances and angles are an average over the cell.

Structural parameter	Experiment hexagonal [74]	Calculation: hexagonal	2 × 2 × 1 supercell with polaron
a	5.04	5.07	10.17
b	5.04	5.07	10.17
c	13.77	13.88	13.93
α (deg)	90	90.0	90.1
β (deg)	90	90.0	90.0
γ (deg)	120	120.0	120.0
z (Fe, 12c)	0.355	0.354	
x (O, 18e)	0.306	0.306	
Fe-O	1.96, 2.12	1.96, 2.11	1.97, 2.12
O-Fe-O	90.5, 86.0	90.9, 86.4	90.6, 86.1
	78.4	78.5	78.3

The calculated bulk structure is used as the basis for computing the ground state configuration for the polaron in a 2 × 2 × 1 supercell, as described above. Listed in Table I are values of the relaxed crystallographic parameters for the polaron ground state in this supercell. Compared with bulk hematite, the formation of the polaron is seen to give rise to a slight expansion of the lattice constants, consistent with the larger size of Fe^{2+} relative to Fe^{3+}. The calculated bond length between the Fe ion with the polaron and its nearest neighbors are found to be distorted relative to the bulk values. Specifically, the nearest Fe ions in the basal plane show three different bond lengths. The shortest bond length with the polaron containing Fe (Fe0) corresponds to the Fe1 ion labeled in Fig. 2(a); the Fe0-Fe1 bond length is 2.92 Å, which is significantly shorter than the average Fe-Fe bond length in the basal plane, which is 2.99 Å. The bond lengths with the Fe ions labeled Fe2 and Fe3 are 0.07 Å larger than that for Fe1, and they do not differ significantly from the bond lengths of 2.99 Å between Fe^{3+} ions far from the polaron. Figure 2(a) also labels the values of the local magnetic moments (**m**) on the Fe ions neighboring the polaron. The Fe1 ion has a significantly smaller magnetic moment than the average magnetic moment of $4.17\mu_B$ for the Fe^{3+} ions, suggesting some delocalization of the polaron charge to this neighboring ion.

B. Activation energies and attempt frequencies

Using a 120-atom 2 × 2 × 1 supercell, we compute saddle-point energies employing the methodology described in the previous section. We compute the activation energy for hopping to Fe1 and Fe2 ions. We will assume that the activation energy barrier for hopping to Fe3 will be similar as that for hopping to Fe2 since the difference between their distance and magnetic moments are insignificant. To identify saddle-point geometries for polaron hopping we begin by generating configurations with atomic positions linearly interpolated between those corresponding to the initial and final polaron sites and then relax the TS, as described in Sec. II A. With a value of $U = 4.3$ eV, we obtain the calculated

TABLE II. Using a Hubbard U value of 4.3 eV, mobilities and activation energies for polaron transport across two different paths to Fe1 and Fe2 show significant differences between the saddle point (column 2) and linear interpolation* (column 3). The next nearest neighbor (NNN) activation energies are also presented.

	μ [cm^2/(V s)]	$\Delta E_{\rm ad}$	$\Delta \tilde{E}_{\rm ad}$ [eV]	τ_0 [THz]
Experiment [75]	0.007	0.17		37
Experiment [45]	0.04	0.118(2)		168.9
Present calc. Fe1	0.009	0.13	0.17	60.4
Present calc. Fe2		0.15	0.24	
Cluster calc. [46]	0.00056*		0.19	18.5
Cluster calc. [14]	0.062*		0.11	99
Present calc. NNN		0.33	0.34	

adiabatic activation energies listed in Table II for hopping to Fe1 and Fe2 ions.

To assess the magnitude of finite-size effects associated with the choice of the 120-atom supercell, we repeated some of the calculations using a 30-atom conventional hexagonal cell (i.e., a $1 \times 1 \times 1$ supercell). For the activation barriers obtained using linearly interpolated atomic configurations ($\Delta \tilde{E}_{\rm ad}$) the value of 0.20 eV obtained with the $1 \times 1 \times 1$ cell compares favorably to the average of the values of 0.17 and 0.24 eV obtained for hops to the Fe1 and Fe2 sites shown in Fig. 1. We note that in the $1 \times 1 \times 1$ cell the activation energies to all neighboring Fe atoms in the basal plane are equivalent by symmetry, whereas the symmetry is broken in the $2 \times 2 \times 1$ supercell. Similarly, the relaxed value of the saddle-point energy ($\Delta E_{\rm ad}$) obtained with the $1 \times 1 \times 1$ supercell is 0.15 eV, which compares well with the values of $\Delta E_{\rm ad} =$ 0.13 eV and 0.15 eV, obtained with the $2 \times 2 \times 1$ supercell for transfer to Fe1 and Fe2 neighbors, respectively. This level of agreement between the $1 \times 1 \times 1$ and $2 \times 2 \times 1$ supercell results for $\Delta E_{\rm ad}$ suggests that the finite-size effects on the calculated activation energies are reasonably small.

The calculated values of 0.13 and 0.15 eV for the activation energy barrier for polaron hopping to Fe1 and Fe2, respectively, compare well with the experimental value of 0.118 eV, which was measured for conductivity within the basal plane of Ti-doped $(Ti_{0.03}Fe_{0.97})_2O_3$ epitaxially grown thin films [45]. Other experimental studies have also reported the anisotropy in the conductivity and activation energy [48,49], finding slightly higher values for the basal plane activation energy than in Ref. [45]. For example, Ref. [49] reports 0.17 eV for the activation energy in the basal plane, compared with 0.74 eV in the [0001] direction. In Ref. [75], measurements on polycrystalline samples yield a lower value for the conductivity, but an average activation energy in all directions of 0.17 eV, equal to the basal plane value in Ref. [49]. Thus our value for the activation energy falls within the range of the smallest value reported for conductivity in the basal plane [45] and the value measured from both a polycrystalline sample [75] and the basal plane of a bulk single crystal [49].

Due to computational cost, the vibrational frequencies in the ground-state and transition-state configurations, which enter the quantum-mechanical expression for the attempt frequency given in Eq. (3), were computed as the Γ-point phonons in the $1 \times 1 \times 1$ supercell of bulk hematite. At the relaxed TS there is an unstable mode of 14.64i THz (488.33i cm^{-1}); the other frequencies are given in the Supplemental Material [76], where results are also given for the rhombohedral primitive cell of hematite and compared to available experimental data [77–81] and other calculations [73,82]. The attempt frequency given in Eq. (3) depends on temperature, and the present calculations give a value at room temperature of $\tau_0 = 60.4$ THz. For comparison, the attempt frequency in the classical limit has a value that is nearly 20 times smaller (2.93 THz). These results thus highlight a strong temperature dependence of the attempt frequency near room temperature, and indicate that the mobility calculated using the classical expression would lead to more than an order of magnitude smaller value for the calculated room-temperature mobility relative to that obtained from Eq. (3).

As shown in Table II, the present calculated value for the attempt frequency is roughly a factor of 3 smaller than the experimental values reported in Ref. [45], but about the same magnitude as the value reported in Ref. [75] for polycrystalline samples. The present calculated values fall between those reported from cluster calculations in Refs. [46] and [14]. Note that the various calculations use different values of the dimensionality in Eq. (4), so direct comparison of the reported mobilities is not possible. Our value of τ_0 contributes to the majority of the discrepancy between our calculation and the experimental 2D basal mobility [45], as reported in Table II and described below.

C. Mobility

With the values of the adiabatic activation energies and attempt frequencies given in the previous subsection, and the average calculated nearest Fe-Fe distance of 2.99 Å for a, we compute a room-temperature basal plane polaron mobility of $\mu = 0.009$ cm^2/(V s). As listed in Table II, this calculated value agrees to within an order of magnitude of the experimental value of 0.04 cm^2/(V s) reported in Ref. [45], obtained for epitaxially grown thin films. The calculated value for the basal plane mobility is very close to that reported in Ref. [75] of 0.007 cm^2/(V s), though a direct comparison is imprecise due to the measurement on a polycrystalline sample.

It should be noted that in computing the mobility from the hopping rates given in Table II, we have assumed that the hopping rates to all nearest neighbors are equal to those reported for Fe1. The difference between the activation energies and hopping rates to Fe1 versus Fe2 and Fe3 is due to the occupation of the electron in a given $t2g$ orbital (d_{yz}). All of the $t2g$ orbitals should be degenerate in a perfect octahedral crystal field, but the lowered symmetry in the defect containing cells leads to a distortion of the octahedra which then lowers the barrier for polaron hopping to one neighbor (Fe1) relative to the other two (Fe2 and Fe3). However, we find that by changing the distortions slightly in the calculations, the polaron can be made to occupy the d_{xy} orbital, which is degenerate in energy. Additionally, changing the distortion and thus the $t2g$ orbital of the nearest neighbors enables the faster electron transfer rate through lowering the activation energy barrier. Thus, since the orbital occupation is expected to vary randomly due to thermal

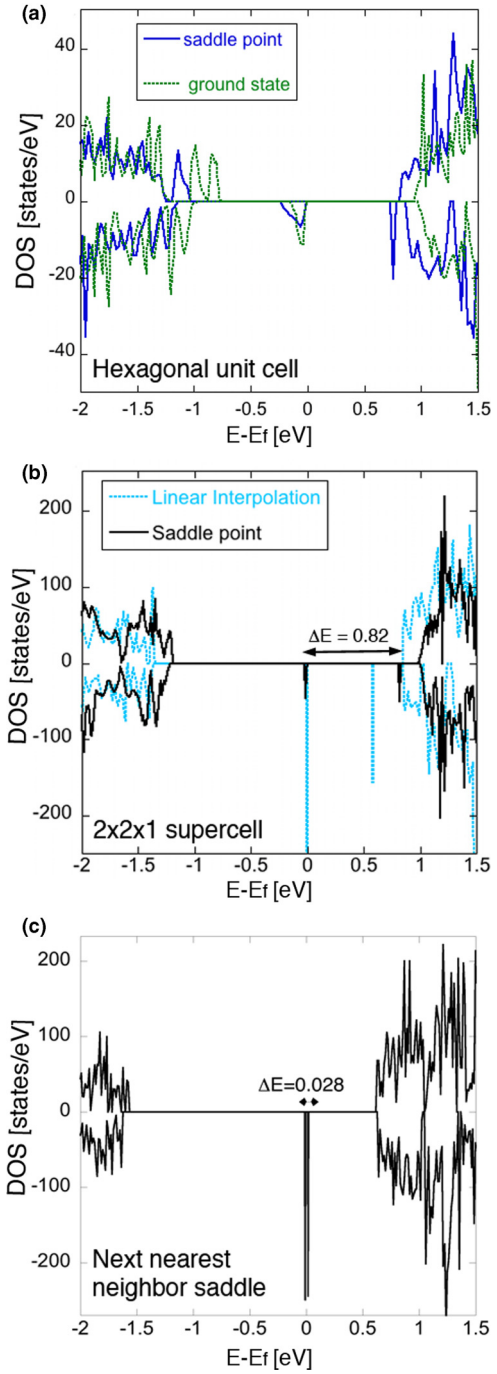

FIG. 3. (Color online) (a) Calculated density of states for a $1 \times 1 \times 1$ unit cell containing an electron small polaron in both the ground-state and saddle-point configurations for nearest-neighbor hopping shows the narrow band due to the polaron in the ground state near the Fermi energy (E_f) in green/dotted lines. At the saddle point, the "bonding" and "antibonding" orbitals are both in the spin-down channel and show appreciable bandwidth (in blue/solid lines). (b) The peaks due to the polaron sharpen in the calculated DOS results obtained with the $2 \times 2 \times 1$ supercell compared to the $1 \times 1 \times 1$ cell for both the linear interpolation (light blue/dashed) and the saddle point (black/solid). (c) Calculated density of states for a saddle-point configuration for hopping to next-nearest neighbors calculated in a $2 \times 2 \times 1$ supercell. The bonding and antibonding defect states are very close together, indicating small electronic coupling, in contrast to the results shown for the nearest-neighbor saddle point.

disorder, we have assumed that all neighbors can be accessed through the faster of the hopping rates given in Table II.

As shown in Table II, the present results for the polaron mobility are found to be in closer agreement with the experimental values reported in Ref. [45] than the previously published calculation by Iordanova *et al.* based on the use of cluster methods, which is a more recent publication than Ref. [14]. Clearly, the large value for $\Delta\tilde{E}_{\rm ad}$ in Ref. [46] contributes to the low estimate of the mobility, but this does not explain why our calculation of μ is so different from that in Ref. [14]. Here, the pre-exponential factor derived in Ref. [14] is roughly 30 times larger than the value calculated in this study. As described above, the temperature-dependent corrections to the preexponential factor considered in the present work are found to have a large effect on the presently calculated mobility.

D. Electronic coupling

We next consider estimates of the electron coupling parameter, through an examination of the electronic structure of the polaron using the Mulliken-Hush formalism, as described in the previous section. Although the $1 \times 1 \times 1$ and $2 \times 2 \times 1$ results for activation energies compare favorably (see above), the electronic structures calculated for polarons in these two supercells show significant differences. Specifically, the defect states associated with the polaron in both the equilibrium and saddle-point geometries are much broader and slightly shifted in the calculations for the $1 \times 1 \times 1$ supercell, relative to the results obtained with the $2 \times 2 \times 1$ supercell, as shown in the calculated electronic density of states (DOS) plotted in Fig. 3(a). Thus, in what follows, the results presented for electronic structure and saddle-point energies will be derived from the larger $2 \times 2 \times 1$ supercell.

In the Mulliken-Hush formalism, the electronic coupling parameter, V_{AB}, is related to ΔE_{12} as in Eq. (5). We estimate in the current work the value of ΔE_{12} from the positions of the defect states in the band gap. For example, Fig. 3(b) shows the calculated DOS in the saddle-point configuration corresponding to hopping from Fe0 to Fe1. The two sharp peaks in the gap are interpreted as the bonding and antibonding states in the Mulliken-Hush formalism. The bonding state is shown in Fig. 2(b), where the charge density from the lower energy peak is plotted in purple. Table III lists values for the coupling parameter V_{AB} derived from the energies of these states. The value of $V_{AB} = 0.41$ eV estimated for hopping to the Fe1 site is larger than $V_{AB} = 0.35$ eV for Fe2, as is

TABLE III. Electronic coupling in eV for polaron transport across two different paths to nearest neighbors Fe1 and Fe2 with $U = 4.3$ eV are compared to cluster calculations and the next nearest neighbor (NNN) results.

	V_{AB}	$\tilde{V}_{AB}$
Present calc. Fe1	0.41	0.29
Present calc. Fe2	0.35	0.23
Cluster calc. [46]		0.190
Cluster calc. [14]		0.204
Present calc. NNN	0.014	0.012

expected due to the delocalization of some of the polaron's charge density over the Fe1 neighbor.

Although it is difficult to derive the magnitude of the electronic coupling parameter from experimental measurements, we can compare the values estimated in the present work with previously calculated values obtained using wave function based methods. Rosso *et al.* [14] calculate $\tilde{V}_{AB}$ to be 0.204 eV for the nearest-neighbor electron transfer in the basal plane, and Iordanova *et al.* [46] calculate $\tilde{V}_{AB}$ to be 0.190 eV using the Mulliken-Hush formula given Eq. (5). These values compare well to our estimate of the electronic coupling at the linear interpolated TS using the Mulliken-Hush formalism, as shown in Table III.

The present and previously published results are in agreement that the electron coupling for nearest-neighbor polaron transfer in hematite is strong, such that the hopping is accurately described as being adiabatic in nature. To test the ability of the present approach to calculate transfer near the nonadiabatic limit, we estimated the magnitude of the coupling for next-nearest-neighbor (NNN) polaron transfer. In Fig. 2(a), the next-nearest-neighbor hop corresponds to transfer from the Fe0 ion to the Fe ion near the **b** lattice vector in the same basal plane, at a distance of approximately 5 Å. From the calculated DOS for the configuration corresponding to the NNN saddle point in Fig. 3(c), we find $V_{AB} = 0.014$ eV, which is smaller than the value estimated by Rosso *et al.* of $\tilde{V}_{AB} = 0.06$ eV [14], but in qualitative agreement with the wave function based approach that the NNN hopping is on the cusp of being nonadiabatic in nature.

IV. SUMMARY

In this work we have employed the formalism of DFT with Hubbard U corrections to compute the activation energies and prefactors for adiabatic hopping of electron small polarons in hematite, α-Fe_2O_3. Employing a Hubbard U value of 4.3 eV, we calculate the value for the room temperature mobility of 0.009 $cm^2/(V\,s)$ that agrees reasonably well with the experimental value of 0.04 $cm^2/(V\,s)$. The calculated activation energies lower gradually with decreasing values of U, but due to the exponential dependence of the mobility of ΔE this leads to a pronounced sensitivity of the mobility values. The work also shows that the use of linearly interpolated geometries for the saddle-point geometry leads to an overestimation of the relaxed adiabatic activation energy by 0.04 eV, which has the effect of lowering the calculated room-temperature values for the electron mobility by a factor of 5.

In addition, we employ the calculated defect energy levels in the saddle-point configuration to estimate the magnitude of the electron coupling parameter in the Marcus theory for electron transport. The results obtained by this approach are found to be in good agreement with those from wave function based methods. Finally, we find it is possible to predict the adiabatic versus nonadiabatic regime of electron transfer in hematite using the electronic structure (DOS) at the saddle point. Our results show that calculating the mobility, adiabatic activation energy, and electronic coupling for polarons on metal ions with DFT + U is a viable method by comparison to experiment and wave function based cluster methods.

ACKNOWLEDGMENTS

This work was initially supported by the Director, Office of Science, Office of Basic Energy Sciences, Materials Sciences and Engineering Division, of the US Department of Energy under Contract No. DE-AC02-05CH11231. N.A.'s final efforts were performed under the auspices of the US Department of Energy by Lawrence Livermore National Laboratory under Contract No. DE-AC-52-07NA27344. Portions of the work of M.A. were supported by Molecularly Engineered Energy Materials (MEEM), an Energy Frontier Research Center funded by the US Department of Energy, Office of Science, Office of Basic Energy Sciences under Award No. DE-SC0001342. J.B.N. is supported by the US Department of Energy, Office of Basic Energy Sciences, Materials Sciences and Engineering Division, under Contract No. DE-AC02-05CH11231. Portions of this work are also supported by the Molecular Foundry through the US Department of Energy, Office of Basic EnergySciences under the same contract number. The authors would like to thank Kevin Hong Ding and Babak Sadigh for their useful discussions on polaron adiabatic and nonadiabatic activation energy calculations and Joel B. Varley and Hannah L. Ray for their clarifying comments.

[1] T. Maxisch, F. Zhou, and G. Ceder, Phys. Rev. B **73**, 104301 (2006).
[2] O. Gerbig, R. Merkle, and J. Maier, Adv. Mater. **25**, 3129 (2013).
[3] H. Kakemoto, Y. Makita, Y. Kino, S. Sakuragi, and T. Tsukamoto, Thin Solid Films **381**, 251 (2001).
[4] H. Ishii, K. Honma, N. Kobayashi, and K. Hirose, Phys. Rev. B **85**, 245206 (2012).
[5] O. F. Schirmer, M. Imlau, and C. Merschjann, Phys. Rev. B **83**, 165106 (2011).
[6] E. Thimsen, F. Le Formal, M. Gratzel, and S. C. Warren, Nano Lett. **11**, 35 (2011).
[7] A. Yildiz, S. B. Lisesivdin, M. Kasap, and D. Mardare, Physica B: Condens. Matter **404**, 1423 (2009).
[8] P. Liao and E. A. Carter, Chem. Soc. Rev. **42**, 2401 (2013).
[9] S.-F. Wang, Y.-F. Hsu, H.-C. Lu, C.-C. Huang, and C.-T. Yeh, Int. J. Hydrogen Energy **37**, 12548 (2012).
[10] Z.-Y. Tian, P. H. Tchoua Ngamou, V. Vannier, K. Kohse-Hoinghaus, and N. Bahlawane, Appl. Catal. B: Environ. **117–118**, 125 (2012).
[11] A. J. Bosman and H. J. van Daal, Adv. Phys. **19**, 1 (1970).
[12] I. G. Austin and M. N. F, Adv. Phys. **18**, 41 (1969).
[13] R. A. Marcus, J. Chem. Phys. **24**, 966 (1956).
[14] K. M. Rosso, D. M. A. Smith, and M. Dupuis, J. Chem. Phys. **118**, 6455 (2003).
[15] P. L. Liao, M. C. Toroker, and E. A. Carter, Nano Lett. **11**, 1775 (2011).
[16] S. Lany and A. Zunger, Phys. Rev. B **80**, 085202 (2009).
[17] V. Alexandrov, A. Neumann, M. M. Scherer, and K. M. Rosso, J. Phys. Chem. C **117**, 2032 (2013).

[18] M. D. Newton, in *Electron Transfer in Chemistry, Volume 1: Principles, Theories, Methods, and Techniques*, edited by V. Balzani (Wiley-VCH, Weinheim, Federal Republic of Germany, 2001).
[19] K. M. Rosso and M. Dupuis, Theor. Chem. Acc. **116**, 124 (2006).
[20] S. Kerisit and K. M. Rosso, J. Chem. Phys. **127**, 124706 (2007).
[21] S. Kerisit, K. M. Rosso, Z. Yang, and J. Liu, J. Phys. Chem. C **113**, 20998 (2009).
[22] F. N. Skomurski, S. Kerisit, and K. M. Rosso, Geochim. Cosmochim. Acta **74**, 4234 (2010).
[23] M. Toroker and E. Carter, J. Phys. Chem. C **116**, 17403 (2012).
[24] J. J. Plata, A. M. Márquez, and J. F. Sanz, J. Phys. Chem. C **117**, 14502 (2013).
[25] S. L. Dudarev, G. A. Botton, S. Y. Savrasov, Z. Szotek, W. M. Temmerman, and A. P. Sutton, Phys. Status Solidi A: Appl. Mater. Sci. **166**, 429 (1998).
[26] M. Cococcioni and S. de Gironcoli, Phys. Rev. B **71**, 035105 (2005).
[27] N. J. Mosey, P. Liao, and E. A. Carter, J. Chem. Phys. **129**, 014103 (2008).
[28] N. A. Deskins and M. Dupuis, Phys. Rev. B **75**, 195212 (2007).
[29] N. A. Deskins and M. Dupuis, J. Phys. Chem. C **113**, 346 (2009).
[30] S. P. Ong, V. L. Chevrier, and G. Ceder, Phys. Rev. B **83**, 075112 (2011).
[31] C. Ouyang, Y. Du, S. Shi, and M. Lei, Appl. Phys. A **373**, 2796 (2009).
[32] T. Van Voorhis, T. Kowalczyk, B. Kaduk, L. P. Wang, C. L. Cheng, and Q. Wu, in *Annual Review of Physical Chemistry, Vol. 61*, edited by S. R. Leone, P. S. Cremer, J. T. Groves, M. A. Johnson, and G. Richmond (Annual Reviews, Palo Alto, 2010), pp. 149–170.
[33] P. Zawadzki, J. Rossmeisl, and K. W. Jacobsen, Phys. Rev. B **84**, 121203 (2011).
[34] K. Gajda-Schrantz, S. Tymen, F. Boudoire, R. Toth, D. K. Bora, W. Clavet, E. C. Graetzel, M. Constable, and A. Braun, Phys. Chem. Chem. Phys. **15**, 1443 (2013).
[35] H. Dotan, O. Kfir, E. Sharlin, O. Blank, M. Gross, I. Dumchin, G. Ankonina, and A. Rothschild, Nat. Mater. **12**, 158 (2013).
[36] F. Zhou and G. Ceder, Phys. Rev. B **81**, 205113 (2010).
[37] H. Peng and S. Lany, Phys. Rev. B **85**, 201202 (2012).
[38] P. L. Liao and E. A. Carter, Phys. Chem. Chem. Phys. **13**, 15189 (2011).
[39] P. Liao, J. A. Keith, and E. A. Carter, J. Am. Chem. Soc. **134**, 13296 (2012).
[40] P. L. Liao and E. A. Carter, J. Appl. Phys. **112**, 013701 (2012).
[41] P. Liao and E. A. Carter, J. Phys. Chem. C **115**, 20795 (2011).
[42] J. Lee and S. Han, Phys. Chem. Chem. Phys. **15**, 18906 (2013).
[43] D. K. Bora, A. Braun, and E. C. Constable, Energy Environ. Sci. **6**, 407 (2013).
[44] X. Meng, G. Qin, W. A. Goddard, III, S. Li, H. Pan, X. Wen, Y. Qin, and L. Zuo, J. Phys. Chem. C **117**, 3779 (2013).
[45] B. Zhao, T. C. Kaspar, T. C. Droubay, J. McCloy, M. E. Bowden, V. Shutthanandan, S. M. Heald, and S. A. Chambers, Phys. Rev. B **84**, 245325 (2011).
[46] N. Iordanova, M. Dupuis, and K. M. Rosso, J. Chem. Phys. **122**, 144305 (2005).
[47] M. Catti, G. Valerio, and R. Dovesi, Phys. Rev. B **51**, 7441 (1995).
[48] D. Benjelloun, J. P. Bonnet, J. P. Doumerc, J. C. Launay, M. Onillon, and P. Hagenmuller, Mater. Chem. Phys. **10**, 503 (1984).
[49] T. Nakau, J. Phys. Soc. Jpn. **15**, 727 (1960).
[50] K. Momma and F. Izumi, J. Appl. Crystallogr. **41**, 653 (2008).
[51] J. D. Tucker, R. Najafabadi, T. R. Allen, and D. Morgan, J. Nucl. Mater. **405**, 216 (2010).
[52] E. De Grave, L. H. Bowen, D. D. Amarsiriwardena, and R. E. Vandenberghe, J. Magn. Magn. Mater. **72**, 129 (1988).
[53] E. Wimmer, W. Wolf, J. Sticht, P. Saxe, C. B. Geller, R. Najafabadi, and G. A. Young, Phys. Rev. B **77**, 134305 (2008).
[54] J. R. Reimers and N. S. Hush, J. Phys. Chem. **95**, 9773 (1991).
[55] W. R. L. Lambrecht, Phys. Status Solidi B **248**, 1547 (2010).
[56] J. P. Perdew, K. Burke, and M. Ernzerhof, Phys. Rev. Lett. **77**, 3865 (1996).
[57] G. Kresse and J. Furthmuller, Phys. Rev. B **54**, 11169 (1996).
[58] G. Kresse and J. Hafner, Phys. Rev. B **47**, 558 (1993).
[59] P. E. Blöchl, Phys. Rev. B **50**, 17953 (1994).
[60] G. Rollmann, P. Entel, A. Rohrbach, and J. Hafner, Phase Transit. **78**, 251 (2005).
[61] Z. D. Pozun and G. Henkelman, J. Chem. Phys. **134**, 224706 (2011).
[62] R. Grau-Crespo, A. Y. Al-Baitai, I. Saadoune, and N. H. De Leeuw, J. Phys.: Condens. Matter **22**, 255401 (2010).
[63] H.-T. Jeng, G. Y. Guo, and D. J. Huang, Phys. Rev. B **74**, 195115 (2006).
[64] Z. Lodziana, Phys. Rev. Lett. **99**, 206402 (2007).
[65] G. K. H. Madsen and P. Novak, Europhys. Lett. **69**, 777 (2005).
[66] A. D. Rowan, C. H. Patterson, and L. V. Gasparov, Phys. Rev. B **79**, 205103 (2009).
[67] M. J. Wenzel and G. Steinle-Neumann, Phys. Rev. B **75**, 214430 (2007).
[68] M. S. Senn, I. Loa, J. P. Wright, and J. P. Attfield, Phys. Rev. B **85**, 125119 (2012).
[69] H. P. Pinto and S. D. Elliott, J. Phys.: Condens. Matter **18**, 10427 (2006).
[70] A. Fujimori, M. Saeki, N. Kimizuka, M. Taniguchi, and S. Suga, Phys. Rev. B **34**, 7318 (1986).
[71] F. Ciccacci, L. Braicovich, E. Puppin, and E. Vescovo, Phys. Rev. B **44**, 10444 (1991).
[72] E. Krén, P. Szabó, and G. Konczos, Phys. Lett. **19**, 103 (1965).
[73] M. Blanchard, M. Lazzeri, F. Mauri, and E. Balan, Am. Mineral. **93**, 1019 (2008).
[74] R. L. Blake, R. E. Hessevick, T. Zoltai, and L. W. Finger, Am. Mineral. **51**, 123 (1966).
[75] B. M. Warnes, F. F. Aplan, and G. Simkovich, Solid State Ion. **12**, 271 (1984).
[76] See Supplemental Material at http://link.aps.org/supplemental/10.1103/PhysRevB.89.245115 for calculated phonons in bulk hematite using DFT+U.
[77] T. D. Glotch, P. R. Christensen, and T. G. Sharp, Icarus **181**, 408 (2006).
[78] S. Onari, T. Arai, and K. Kudo, Phys. Rev. B **16**, 1717 (1977).
[79] S. H. Shim and T. S. Duffy, Am. Mineral. **87**, 318 (2002).
[80] I. R. Beattie and T. R. Gilson, J. Chem. Soc. A: Inorg. Phys. Theor. 980 (1970).
[81] A. U. Gehring and A. M. Hofmeister, Clays Clay Miner. **42**, 409 (1994).
[82] I. Chamritski and G. Burns, J. Phys. Chem. B **109**, 4965 (2005).